Distributed pressure sensing based flight control for small fixed wing UAS

Kieran T. Wood, Sergio Araujo-Estrada, Thomas Richardson, and Shane Windsor
Department of Aerospace Engineering, University of Bristol, Bristol, BS8 1TR, UK

Small fixed-wing Unmanned Aerial Systems (UAS) might require increased agility when operating in turbulent wind fields. In these conditions, conventional sensor suites could be augmented with additional flow-sensing to extend the aircraft's usable flight envelope. Inspired by distributed sensor arrays in biological systems, a UAS with a chord-wise array of pressure sensors was developed. Wind-tunnel testing characterised these sensors alongside a conventional airspeed sensor and an angle-of-attack (AoA) vane, and showed a single pressure measurement gave a linear response to AoA pre-stall. Flight tests initially manually piloted the vehicle through pitching manoeuvres, then in a series of automated manoeuvres based on closed-loop feedback using an estimate of AoA from the single pressure port. The AoA estimate was successfully used to control the attitude of the aircraft. An Artificial Neural Network (ANN) was trained to estimate the AoA and airspeed using all pressure ports in the array, and validated using flight-trial data. The ANN more accurately estimated the AoA over a single port method with good robustness to stall and unsteady flow. Distributed flow sensors could be used to supplement conventional flight control systems, providing enhanced information about wing flow conditions with application to systems with highly flexible or morphing wings.

I. Introduction

Small Unmanned Air Systems (UAS) flying at low levels in urban areas require high manoeuvrability to fly within confined streets. They also have to cope with a complex aerodynamic environment with high levels of turbulence, with air speed possibly fluctuating rapidly by more than 40% at rooftop altitudes [1]. Current control systems for small UAS typically make use of several traditional sensors. Namely a 6-degree-of-freedom (DoF) inertial measurement unit (IMU), a GPS receiver, a magnetometer, an anemometer, and possibly an altimeter [2]. These avionics systems are well developed and work well for flight in simple conditions. When trying to stabilise a small UAS in challenging gusty conditions, however, these sensors may not provide all the information required to make use of the full aircraft's flight envelope. For example, a short term gust might cause a temporary change in angle of attack (AoA) and induce stall on the wings, however the flight control system will not react until the flow has separated from the wing leading to a loss of lift resulting in a inertial disturbance as measured by the IMU or altimeter.

A potential method for enhancing UAS flight control performance is to directly measure the airflow around the wing and use information about the state of the airflow as an input to the flight control system. This principle of measuring distributed flow information appears to used in many biological flyers; birds sense airflow on their wings using mechanosensors [3], bats use flow sensitive hairs in a similar way [4], and insects also have large numbers of flow sensitive hairs [5]. A variety of different man-made sensors have also been used to measure the distribution of flow properties on the wings of small UAS. The most common are pressure sensors [6–12], but more novel sensors such as hotfilms [13, 14] and artificial hair sensors [15, 16] have also been used to measure flow velocity.

There are a number of potential benefits of using distributed flow sensing as part of the flight control of a small UAS:

- *Extension of flight envelope* - Most flight control systems for small UAS are based around a linear flight dynamics model. The validity of this linear model will break down when pushing the aircraft to the edges of its possible flight envelope, e.g. stall conditions. By using direct measurements of flow around the wings it may be possible to operate in more non-linear flight regimes. For example, maintaining non-stalled flow around the wings, or exploiting a controlled stall for more extreme manoeuvres.
- *Flexible wing control* - Aircraft with highly flexible wings, or morphing wings with high DoF, could benefit from distributed flow sensing, using local flow information to tailor the flow state and associated loads over different sections of the wing.
- *Early detection* - Having a distributed array of sensors may allow the earliest stages of gusts to be detected as a flow disturbance moves across the array. Suitable control can then be implemented to mitigate the developing effect of the gust. [17]
- *Faster response* - The total moment, and therefore angular acceleration, of the aircraft can be estimated by integrating the airflow measurements over the surface of the aircraft. This in theory allows a faster response to disturbances in attitude which are normally measured as changes in angular rate using an IMU [18].
- *Damage tolerance* - Flow sensors mounted within the wing structure could be more robust to damage, when compared to probes and vanes, or other vulnerable externally mounted sensors.

Previous studies using distributed flow sensors in the wings of small UAS have shown that these arrays can be used to measure parameters such as airspeed (V), angle of attack (AoA), and side-slip angle [6, 8, 11, 13, 14]. These are similar to the measurements provided by the instruments on a conventional air-data boom, but with the advantage of reduced cost and increased damage tolerance [6]. It has also been demonstrated that wing mounted arrays can be used to estimate non-conventional parameters such as lift, drag and pitching moment [15, 16]. These estimates could potentially be used in a physics based control approach where the total forces and moments acting on the aircraft are estimated based on signals from distributed sensors [19].

In this study we developed a small UAS system with a chord-wise distributed array of pressure sensors in the wing. Wind tunnel testing was then used to characterise these sensors alongside a conventional airspeed sensor and an AoA

vane. The same fixed wing UAS was then flight tested, firstly manually piloted through a series of pitching manoeuvres, then in a series of automated manoeuvres based on closed loop feedback using an estimate of AoA from a single pressure port. Post-processing of wind tunnel and flight testing data was then used to train an ANN to estimate the AoA and V of the UAS based on signals from all of the pressure ports in the array. This study extends previous work by demonstrating the feasibility of using pressure sensors for attitude control during outdoor flight testing, as well as demonstrating the ability of distributed pressure arrays to be used to estimate AoA and V under stall conditions.

II. System Description

This section gives details of the complete UAS comprising; a base flight platform, traditional autopilot avionics, additional pressure sensing electronics, and a ground station with a pilot. The overall system architecture is shown in Fig. 1. The same system was used for both wind tunnel testing and outdoor flight testing. The additional pressure sensing sub-systems comprised: the rapid-prototyped wing insert, a set of pressure transducers, and a micro-controller. This sub-system passed wing pressure valued directly to the auto-pilot. Note there are two sources of data logging available; the pressure sensor system micro-controller is storing raw analogue samples at 200 Hz and the auto-pilot logs a variety of measurements (for example airspeed, GPS location, and pitch angle) between 10 Hz and 25 Hz.

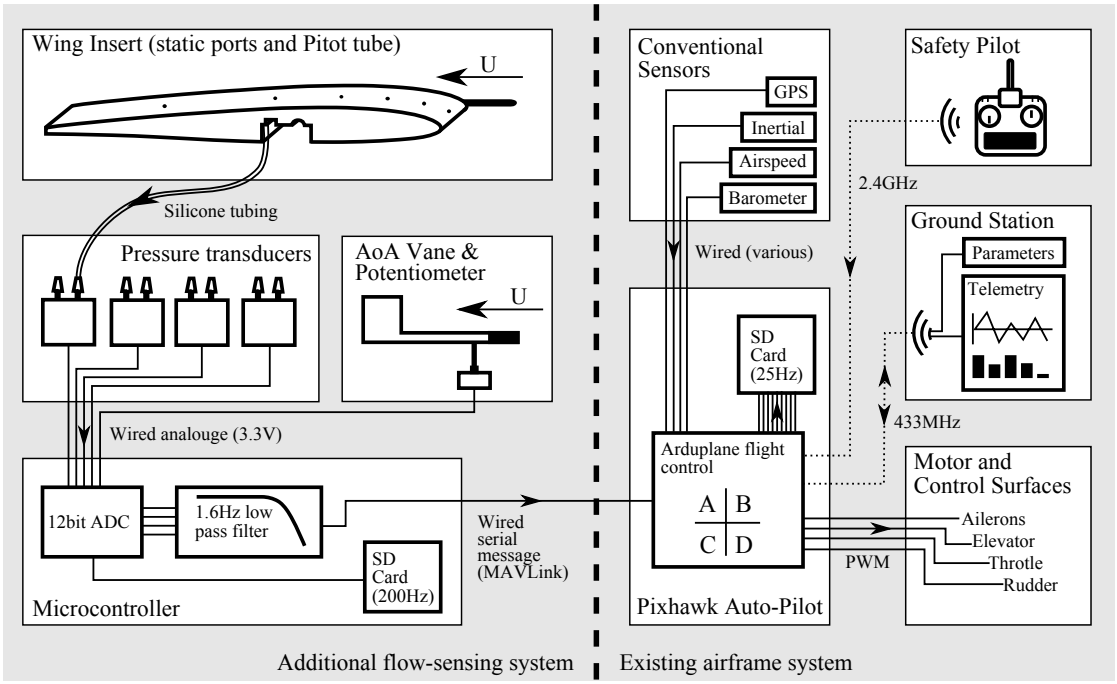

Fig. 1 Aircraft control system architecture.

A. Flight Vehicle

The focus of this investigation was the integration and utilisation of pressure sensors for longitudinal control of a small UAS, and not the development of an entirely new airframe, hence the platform chosen was a recreational model plane (Bixler-2, Hobbyking, UK) as shown in Fig. 2. This UAS is a battery powered, high wing, push propeller, model aircraft with dimensions given in Table 1. It is mostly constructed from Expanded PolyOlefin (EPO) with structural stiffening provided by a carbon tube main wing spar, and a carbon rod running along the tail boom. For this reason the airframe can be modified easily with basic construction methods to embed additional sensors in the wings and avionics within the main body. The original vehicle has four sets of servo actuated control surfaces: elevator, rudder, ailerons, and flaps. Note however, the modifications for the pressure sensors removed the ability to use the flaps. Thrust is provided by a 7"×5" propeller driven by small brushless motor with a 20 A electronic speed controller (ESC). From previous research experience [20], the unmodified vehicle is comfortably capable of carrying approximately 400 g of additional payload at flight speeds of approximately 15 m s^{-1}. In Fig. 2, the additional wing pressure sensors insert can be seen in the starboard wing, with all other additional avionics contained within the fuselage. The secondary Pitot tube is mounted adjacent to the wing insert. The angle-of-attack sensor is mounted on the port side of the nose.

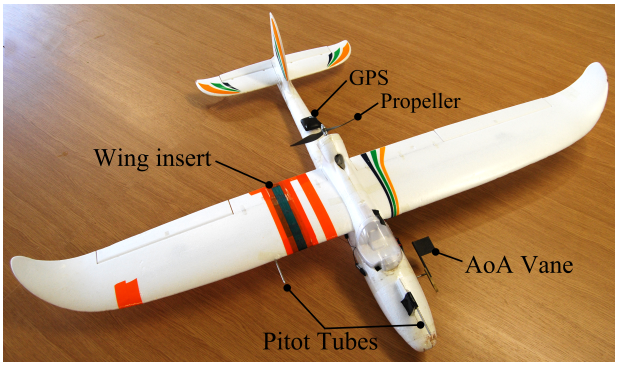

Fig. 2 The modified aircraft.

Table 1 Airframe main characteristics

Parameter	Value
Mass (airframe only)	0.760 kg
Mass (total w/o battery)	0.975 kg
Mass (total with battery)	1.175 kg
Wing span	1.500 m
Wing chord	0.198 m
Wing area	0.242 m^2
Length	0.963 m
Wing loading	47.677 N m^{-2}
Cruise Speed	15 m s^{-1}
Aspect Ratio	7.6

B. Flight Control System

The vehicle was equipped with a core set of avionics to enable fully automatic flight, including take-off, way-point following, longitudinal manoeuvring, and landing. The automation of all flight segments made the outdoor flight testing both reliable and repeatable. The core flight control systems comprised a flight computer (Pixhawk by 3DRobotics, USA), GPS & magnetometer unit (UBlox NEO-7 GPS, 3DRobotics, USA), and telemetry radio module (SiK Radio v2, 3DRobotics, USA). The vehicle was also equipped with a digital Pitot tube dedicated to the flight computer. The flight computer acted as an autopilot and used a traditional IMU for roll/pitch/yaw stability, while updating servo commands at 50 Hz. Is also has an additional TTL serial interface operating with 3.3 V logic levels which was used for a direct interface to the pressure sensing micro-controller.

A pilot safety link comprised a radio receiver (X8R, FrSky, China) and a transmitter (Taranis X9D-Plus, FrSky, China). The safety link allowed a human pilot to reliably issue commands to initiate and cancel experimental modes to the autopilot, and also assume manual control of the vehicle at any time. The entire system was powered from a 3S 2000 mA h lithium polymer battery (Nanotech, Turnigy, China). Two independent 5 V power regulators were used for the auto-pilot and the additional avionics to ensure any problems with the experiential hardware could not interfere with the core flight control. With the additional weight and power requirements of the pressure sensing system, the maximum flight duration was approximately 12 min.

C. Pressure Sensing Array

To enable the direct measurement of the wing surface static pressure, an insert was created to hold a chord-wise array of pressure tappings aligned perpendicular to the surface. The wing insert, shown in Fig. 3, was created from Polylactic Acid (PLA) thermoplastic using a rapid prototyping method. It was designed to match the aerodynamic cross-section of the aircraft wing at approximately the quarter span, whilst also allowing space for pressure tubing and an attachment to the main spar. Holes were also added for carbon rods which acted as partial span spars to improve strength and stiffness around the insert. The insert was 45 mm wide, full chord, and completely rigid, hence the trailing edge flap became permanently fixed in position. The insert was installed on the starboard wing at 0.15 m (20% semi-span) from the wing root as shown in Fig. 2. This arrangement of sensor ports allowed the pressure distribution to be measured where the flow was likely to be minimally affected by the wing tip vortex, giving a good representation of the flow over the inboard portion of the wing from which aerodynamic parameters such as AoA could be estimated. Additional inserts could be used in the future to measure the spanwise pressure distribution if required.

A total of seven pressure tapping points (p_{1-7}) were added to the insert; six on the upper surface at 3, 10, 20, 30, 50, 75% chord, and one on the lower surface at 10% chord. The pressure ports were created from 1 mm ID brass tubes bonded to the outer wall of the insert and then trimmed flush with the surface. The free end of the brass tubes extended a short distance into small voids within the structure to allow for the attachment of silicone tubing. In addition to the static

pressure ports, a Pitot tube (p_8) was installed in the vicinity of the insert such that a local airspeed could be calculated without having to modify the Pitot tube dedicated to the flight computer.

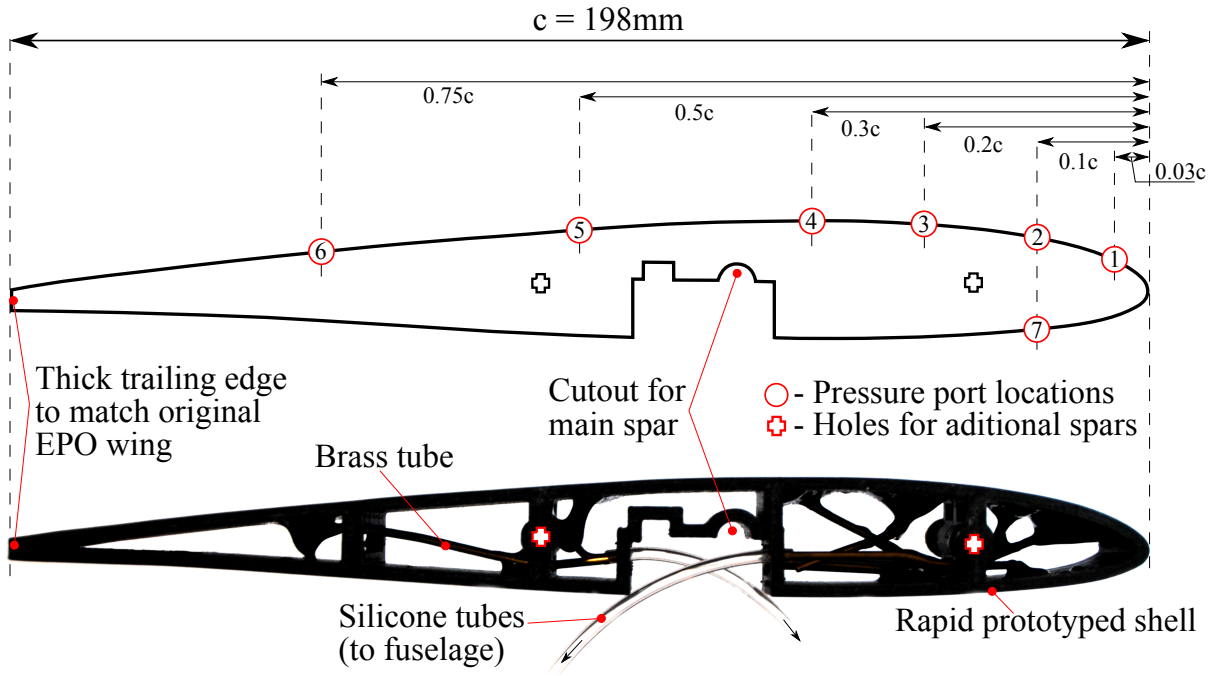

Fig. 3 Rapid prototyped wing insert and diagram showing the chord-wise potion of the pressure ports.

D. Pressure Transducers

The pressure ports were connected to pressure transducers located in the aircraft fuselage via short lengths of silicone tubing. The internal space allowed for the mounting of two custom PCB boards, each holding four pressure transducers. Seven of the pressure transducers were connected to static ports p_{1-7}, leaving the reference pressure side unoccupied. Therefore the static surface pressure on the wing was relative to the static pressure within the fuselage. Since this volume was not sealed, the sensed pressure varied with external pressure. Both connections of the eighth pressure transducer were connected to the wing Pitot tube.

The selected pressure transducers (MPXV7002, Freescale) measuring range is ±2 kPa, with a maximum output error equal to 6.25% of the full measuring span. The transducers output an analogue voltage proportional to the differential pressure with a gain of 1 V kPa^{-1} and an offset of 2.5 V. Therefore the normal output varied over the range 0.5 V - 4.5 V. Custom PCB boards were used to mount the transducers, providing each transducer with power and scaling the analogue output using a potential divider to be within the range of the micro-controller electronics.

E. Micro-Controller

A micro-controller development board (Teensy3.6, PJRC) was used to sample, store, and forward the pressure information to the auto-pilot. In addition to the eight analogue signals from the pressure transducers, the micro-controller was also used to sample the angle of attack sensor and supply voltage; hence a total of 10 channels were sampled at 200 Hz. These values are stored raw on the local SD card and a subset of filtered data was forwarded to the auto-pilot via a wired serial link. The filter was a first-order low-pass design implemented at 200 Hz with a bandwidth of 1.6 Hz. A common timestamp was shared between the Teensy and auto-pilot such that the higher rate SD card data could be aligned with the standard Pixhawk telemetry log files.

F. Angle-of-Attack Vane

An AoA sensor was used to provide an additional source of ground truth information as AoA is not directly measured by conventional auto-pilot sensors (inertial, barometric, airspeed, and GPS). The angle of attack sensor comprised a balanced wind vane (Fig. 2) and a single turn precision potentiometer (157S103MB9002, Vishay). This potentiometer can rotate an infinite number of turns, however the resistance varies between between 0 and the 10 kΩ maximum once per revolution. The components were installed on the side of the fore-fuselage to ensure the vane was exposed to almost free-stream flow.

III. Wind Tunnel Testing

A series of wind tunnel tests were performed to characterise the relationship between surface pressure measurements and AoA. At the same time the vane based AoA sensor and wing mounted Pitot tube were also calibrated. The airframe was rigidly fixed atop a servo actuated mount and installed in the University Of Bristol Open-Jet Wind Tunnel at as shown in Fig. 4. The mount has the ability to automatically orientate the model over a range of incidence angles, and since the model was fixed in all translational axes, the pitch and the AoA become equivalent. For all tests the control surfaces were set to neutral positions and the main motor was disabled. The range of airspeeds was $U_s = [8, 10, 12, 14, 16]\,\mathrm{m\,s^{-1}}$ which covered the nominal cruise speed of $15\,\mathrm{m\,s^{-1}}$ and the lower speeds expected when operating at higher angle-of-attack.

The characterisation comprised a sweep of pitch angles from $-4°$ to $16°$ (step size $2°$ from -4 to 6, then $1°$ steps) over a range of airspeeds. A script was created to automatically step through a range of pitch angles with a short pause at each to collect pressure samples. Note that although the demanded pitch angles were set to integer values, the actual pitch of the aircraft covers a non-uniform distribution due to non-linearities in the actuation system and backlash in the mechanism. For this reason the auto-pilot inertial sensor was used as the pitch measurement.

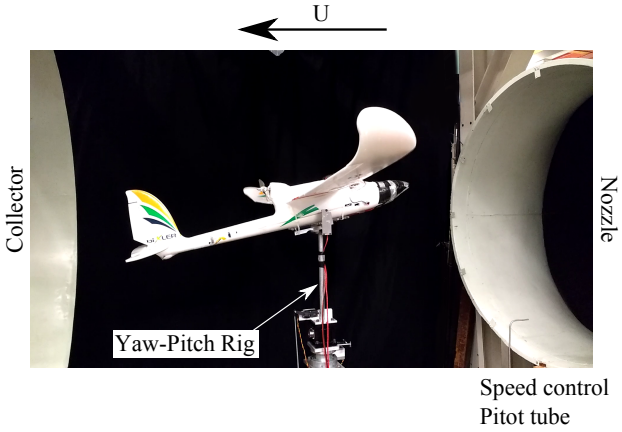

Fig. 4 Flow sensing airframe installed in University of Bristol Open Jet Wind Tunnel

A. Sensor calibration

Both the wing Pitot tube and AoA vane were calibrated during the wind tunnel tests. The wing Pitot tube was characterised by comparing the measured differential pressure with airspeed measured by the pre-calibrated auto-pilot sensor over air speeds from $8\,\mathrm{m\,s^{-1}}$ to $16\,\mathrm{m\,s^{-1}}$. The AoA vane was calibrated against the gravity referenced pitch measurement from the IMU.

The data collected from the static pressure ports was analysed to identify the relationship between pressure measurements on the wing surface and AoA. The pressure measurements for pressure port 1 are shown in Fig. 5a over the range of airspeeds and AoAs; from this the stall angle is identified to be approximately 12°. Another noticeable feature is the near zero differential pressure at −3° AoA which suggests the stagnation point is close to the 3 % chord location on the upper surface. For AoA below 12° there is a monotonic relationship between the wing surface pressure and AoA, however there is also a dependence upon airspeed. To remove this dependence and create a more reliable AoA measurement, the pressures are normalised using the airspeed measurement from the wing Pitot tube (${V_w}^2$). Figure 5b shows the same data after it has been normalised by a factor of $q = 0.5\rho {V_w}^2$, where the air density is assumed constant at $\rho = 1.225\,\mathrm{kg\,m^{-3}}$. The normalisation has made the coefficient of pressure invariant to airspeed, hence there is now a linear relationship between C_{p_1} and AoA up to 10°. It was not possible to completely remove the airspeed dependency for the pressure measured from ports 2 to 7. As the measured pressure from these ports was within the sensor's maximum error region, it is likely that the observed airspeed dependency was a measurement error effect.

It should be noted that by only using the signals from a single pressure port a lot of potentially useful information is lost. An alternative is to feed the full sensing array information into an ANN and train it to learn an appropriate model to estimate the angle of attack. This approach is presented in Section IV.C.

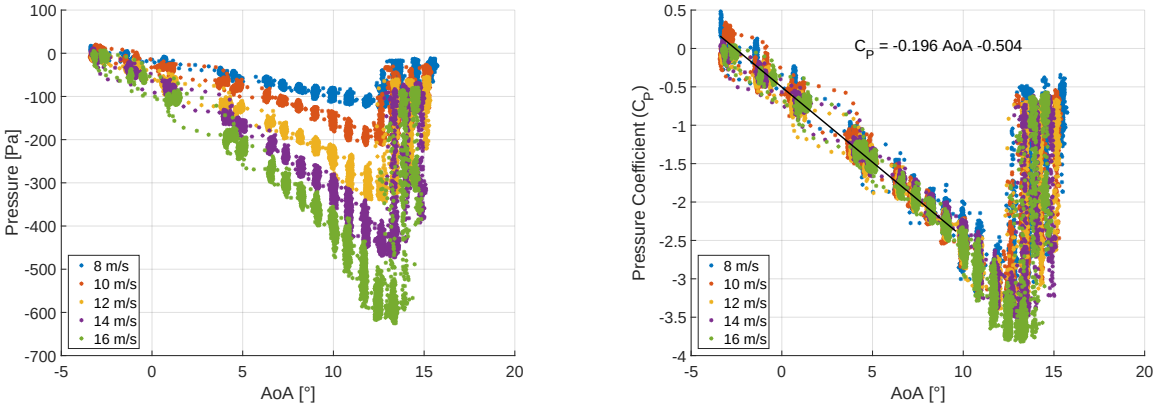

(a) Pressure

(b) Pressure Coefficient

Fig. 5 Wing pressure and pressure coefficient for pressure port 1 at various AoAs and airspeeds.

IV. Outdoor Flight Testing

The outdoor flight campaign was conducted in a sequential manner to build up an understanding of how the longitudinal control of a small UAS could be augmented with real-time wing pressure information. By design, the vehicle tested in the wind tunnel was fully airworthy and could be flown outdoors without modification. The initial flights were conducted to collect data for analysis of both cruise and stall behaviours. Follow-on flights sought to replace the inertial pitch sensor with the pressure based AoA measurement for closed-loop flight control.

A. Flying Site

All experimental work was conducted at the University of Bristol outdoor flight test facility as shown in Fig. 6. An automatic waypoint mission was created to fly the vehicle in a racetrack pattern with each test comprising several laps:

1) From the take-off point the vehicle ascended to a target altitude of 80 m over the duration of a single lap.
2) The vehicle then maintained altitude and speed for several laps whilst experiments were conducted on the upwind leg.
3) During the final lap, the vehicle descends and lands.

The track was set to have straight lengths of 120 m which was a compromise between allowing the vehicle to straighten out after the turns, whilst also keeping the vehicle close enough that a pilot could safely take command in unexpected situations. The track was orientated such that one of the straight legs was directly into the wind. A diagram of the waypoints is shown in Fig. 6. The racetrack waypoint path is shown with the take-off (green circle) and landing (red square) points. The experimental pressure based control tests were conducted along the 120 m upwind leg only. The cruise speed was set to 15 m s^{-1} at all times.

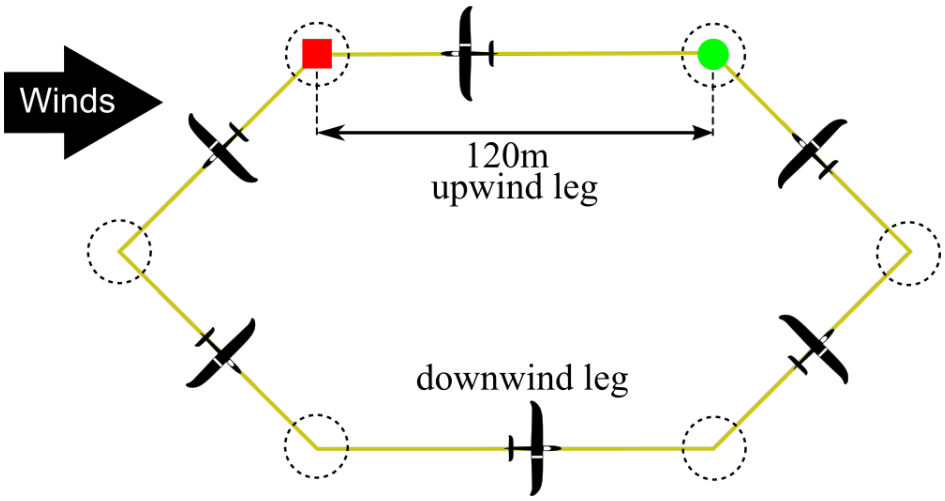

Fig. 6 UoB outdoor experimental flight facility located at Fenswood Farm (51.423322N, 2.671129W).

B. Closed-loop Angle of Attack Control

The outdoor experimental data comprises a mix of manual and automatic flights. During the manual flights, all degrees of freedom were under the direct control of the pilot. In the automatic flights, the auto-pilot system was responsible for stabilisation and navigation, including take-off and landing. The stock autopilot code (ArduPlane version 3.7.1) was modified to include an experimental mode whereby the elevator and throttle control could be temporarily altered as detailed in Fig. 7. The stock fly-by-wire (FBW) pitch control is normally updated with an error between the Attitude and Heading Reference System (AHRS) pitch angle and the desired pitch angle from the navigation controller. When the experiment mode is active, this error is replaced with the difference between the pressure based AoA measurement and a pre-set ramp function. Simultaneously, the throttle was also set to a constant value. The pressure based AoA measurement used the AoA estimate based on the identified linear relationship between the coefficient of pressure at pressure port 1 and AoA.

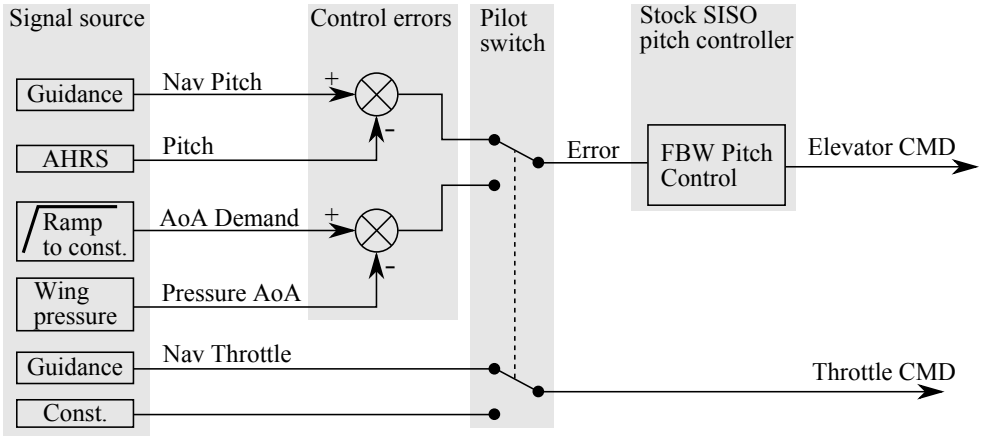

Fig. 7 The structure of the experimental AoA control.

C. Estimation Using Neural Networks

Following wind tunnel and outdoor flight testing, a series of feed-forward Artificial-Neural-Networks (ANN) were trained to estimate the AoA and airspeed of the UAS using data from all of the pressure ports. The training was carried out by combining all of the wind tunnel data sets and four outdoor test flights. Both wind tunnel and test flight data were used in order to improve the estimation performance of the ANN, as the airspeed range and testing conditions (e.g. turbulence, atmospheric conditions) between data sets were different. The estimation performance was validated using four outdoor flights data sets independent from those used in training.

Figure 8 shows the general structure of the ANN used for estimation of the AoA and airspeed. Each ANN consisted of three main layers; an input, hidden, and output layer. The input layer scaled the pressure sensors inputs based on the mean values and range of the expected inputs. The neurons in the hidden layers used hyperbolic tangent sigmoid functions as activation functions. The output layer scaled the signals produced by the hidden layer to match the magnitude of the target function. The AoA and V readings were used as target functions using the pressure signals from all wing ports as inputs. 32 ANNs with a range of different structures were trained to estimate either the AoA or V. The sum of the Mean-Square-Error (MSE) for training and validation was used as selection criteria to find the ANN that best fitted the data. The ANN were trained using MATLAB Version 9.2 and Neural Network Toolbox Version 10.0, Release 2017a (The MathWorks, Inc., Natick, Massachusetts, United States), employing the Levenberg-Marquardt backpropagation algorithm as the training function. The resulting ANNs for both AoA and airspeed estimation each have 3 hidden layers, with 17 neurons in total for AoA estimation (7 in the input layer; 5, 3 and 1 in the hidden layers; and 1 in the output layer) and 21 neurons in total for V estimation (7 in the input layer; 7, 5 and 1 in the hidden layers; and 1 in the output layer).

V. Results

A. Manual Flight

The initial flights were conducted to log and assess the quality of the pressure measurements under typical outdoor free-flight conditions. An experienced pilot manually guided the aircraft in the racetrack pattern including two deliberate stall manoeuvres achieved by gradually reducing the throttle whilst simultaneously applying nose-up elevator commands until the vehicle could not maintain flight.

Figure 9a shows the time-histories for the two airspeed measurement methods and three AoA measurement methods over a period of trimmed flight. The airspeed measured by the wing Pitot tube was calculated based on the wind tunnel calibration. There was generally a good correlation between the two airspeed measurements with a RMS error between the signals of $0.40\,\mathrm{m\,s^{-1}}$ for the period shown. The vane AoA and single pressure port based AoA (for port p_1) were also calculated using the relationships identified in the wind tunnel, while the ANN-based AoA was computed using the

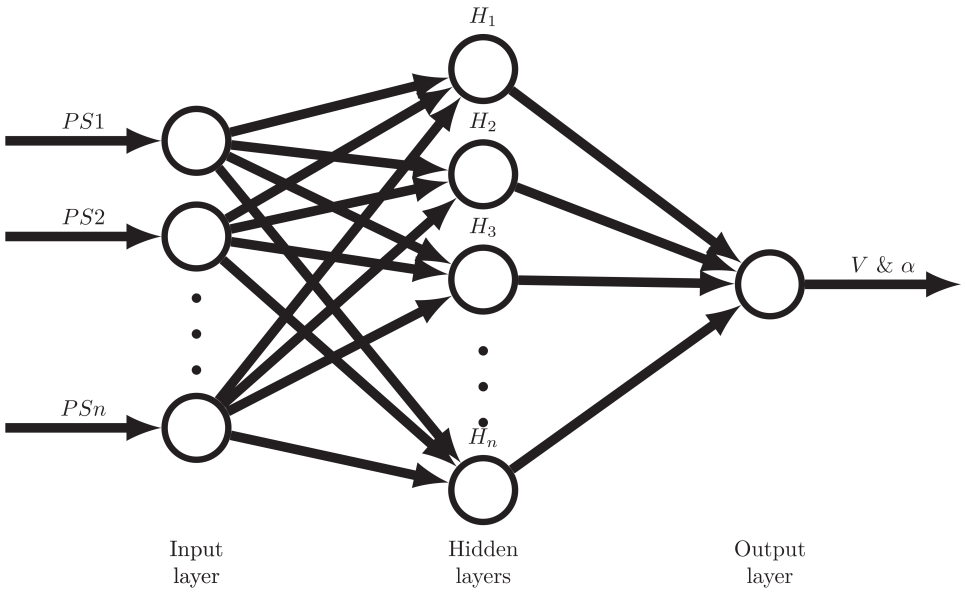

Fig. 8 General structure of ANN used for estimation of angle of attack and airspeed based on input from pressure sensor (PS) data.

ANN described in Section IV.C. The vane AoA and ANN AoA measurements matched well, with many of the same transient features appearing in both sets of data with similar magnitudes. The RMS error of the ANN AoA estimate was 1.05° compared to the AoA vane. The single pressure port based AoA measurement reproduced the transient features well, although the agreement with the vane AoA was not as good as that of the ANN AoA, with a noticeable offset resulting in an RMS error of 2.86°.

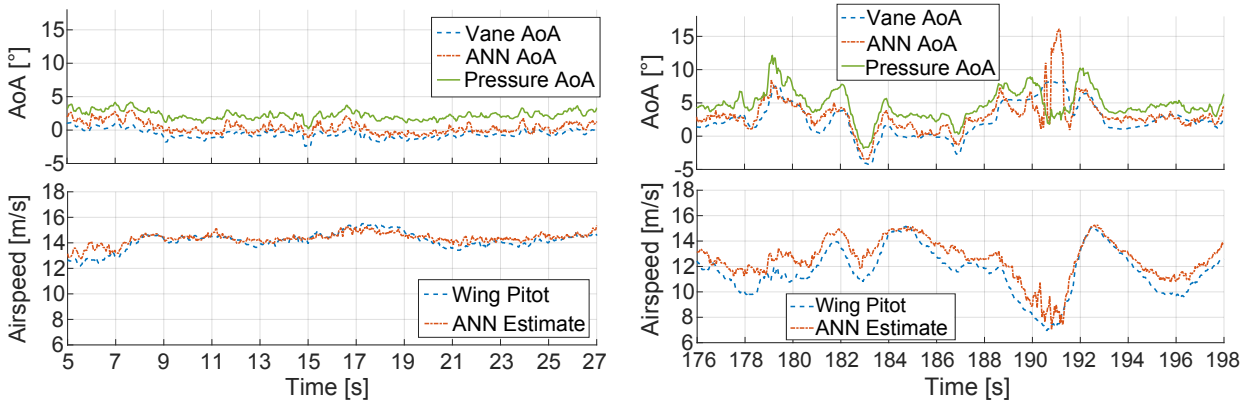

(a) Straight and Level

(b) Stalling

Fig. 9 Airspeed and angle-of-attack measurements during manually piloted flight. ANN estimates are shown for validation flight data.

Later during the same flight, two stall manoeuvres were attempted with the telemetry data shown in Fig. 9b. At approximately 190 s the aircraft entered a full stall as indicated by the AoA measurements temporarily diverging and V

dropping. Shortly after the stall, the pilot recovered to level flight and the three AoA measurements converged. Earlier in the flight (179 s) another stall manoeuvre was attempted, however in this case a full stall did not develop; this can be attributed to the airspeed remaining significantly higher. Although now showing poorer accuracy than in straight and level flight, the ANN-based AoA measurement remained accurate within an RMS error of 1.78° even during the large airspeed fluctuations. Even though the single pressure port based AoA measurement tracked the main transient features, the RMS error increased to 2.91°. This was not unexpected as the single pressure port based AoA calibration was only valid for AoA up to 10°.

B. Normalized Pressure-Based AoA Feedback in Cruise

A series of experiments were conducted to assess the ability to directly control the AoA of the vehicle using wing flow sensing. Using the experimental control structure (Fig. 7) with a ramp rate of $2\,^{\circ}\,s^{-1}$, the aircraft was commanded to fly at 6° and 8° AoA with representative time-histories shown in Fig. 10a and Fig. 10b respectively. Vertical lines representing the time bounds of when the vehicle was under closed-loop control have been overlaid. For the 6° demand case, the vehicle successfully increased its AoA and achieved a new steady state at the desired set-point for approximately 10 s. At the end of the experimental period was a sudden jump in AoA as the vehicle automatically recovered to the original flight path. The start of the 8° AoA case begun similarly, however at approximately 218 s there was a sudden additional elevator command. This briefly stalled the wing as indicated by the drop in AoA to 5° despite a nose up elevator command. The vehicle then entered an unstable oscillation with repeated stalls. The event was attributed to a gust as indicated by the gyro measurements immediately before the elevator command. Based on this behavior, the remaining AoA control experiments were conducted with a maximum 6° demand. Note that the controller gains used for these experiments were designed for inertial feedback control, which is less tolerant of atmospheric perturbations and that this AoA demand limit could be relaxed with more appropriate control tuning. The 6° case showed the potential advantages of directly controlling the AoA using flow sensing. For instance, as the throttle was set to 80 %, the vehicle increased altitude due to the additional wing lift, even when the airspeed decreased to approximately $8\,m\,s^{-1}$. This suggests that the throttle could be used for controlling the rate of climb. An example of this application is discussed further in Section V.C.

Since the vehicle had not visually stalled, the ramp rate was increased to $4\,^{\circ}\,s^{-1}$ with a demand of 20° AoA to ensure a stall event within the up-wind leg of the circuit. The test was repeated and the results are shown in Fig. 11. In this case the elevator demand quickly saturated and a stall occurred at approximately 9° AoA. The vehicle then enters an oscillatory motion, exchanging speed and altitude. This confirmed that for outdoor conditions, the tolerable AoA without stall was lower than in the wind-tunnel environment.

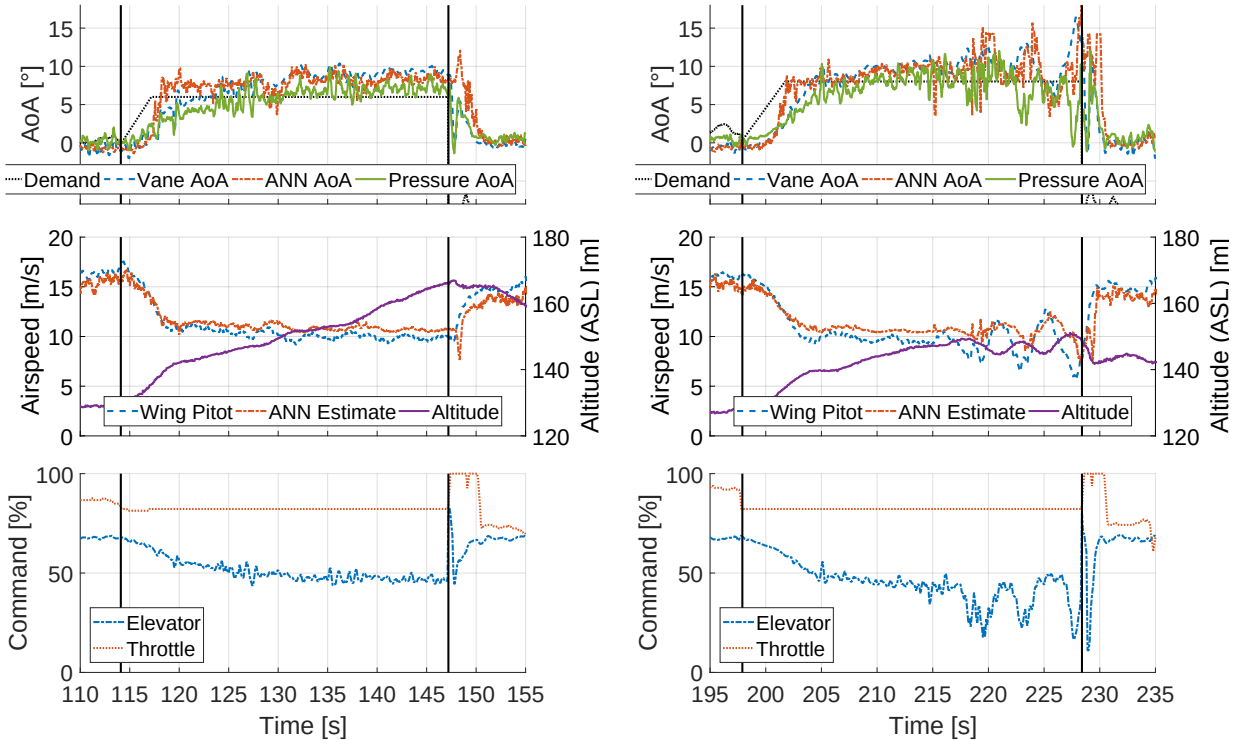

(a) AoA = 6°

(b) AoA = 8°

Fig. 10 Various signals from 6° and 8° AoA flight. ANN estimates are shown for validation flight data.

C. Climb rates

To assess the performance benefits of flying at a set AoA, a series of tests were conducted with various throttle limits between 0 and 100%. In each case the vehicle was set to use the AoA feedback control and fly at 6°. Depending on the throttle, the vehicle would either ascend or descend. For each case the climb rate and airspeed were extracted for a short section of flight after the vehicle had achieved the demanded AoA. Figure 12 shows the linear relationship between the throttle percentage and the flight path angle (γ), this shows that for this vehicle a throttle setting of approximately 50% is required for level flight.

D. ANN Performance

The ANN's were trained based on the wind tunnel data and four outdoor flight tests, with four different flight tests used for validation. The RMS error statistics for both the angle of attack and airspeed estimation are given in Table 2. The angle of attack estimation error distribution for the wind tunnel data set is shown in Fig. 13a. The error distribution for the vane, ANN and single pressure sensor AoA estimation were very similar. However, the single pressure sensor

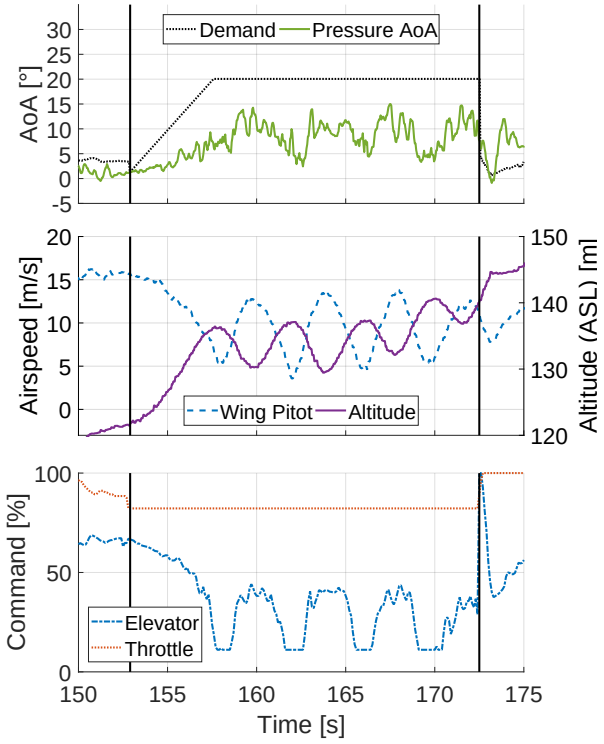

Fig. 11 Various signals from a deliberate stalling flight.

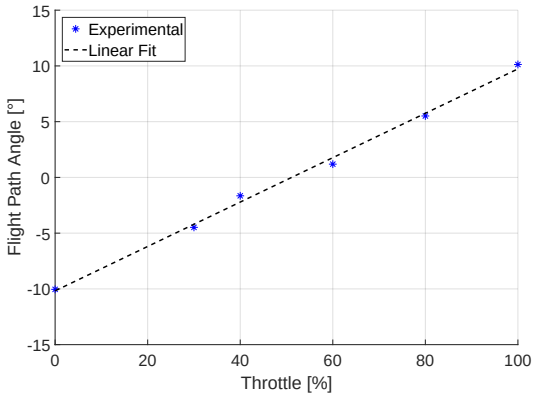

Fig. 12 Throttle vs. flight path angle (γ) for a fixed 6° AoA. Effectively the throttle becomes responsible for controlling the rate of climb.

error spread well into the 12° region implying that is was sometimes significantly under-predicting. Looking at the relationship between AoA and estimation error (Fig. 14a) shows that before the stall region the three methods gave comparable estimation error. But after stall (AoA $> 12^\circ$) the single pressure sensor based estimation error increased significantly. For the outdoor flights data set (Fig. 13b), the mean and standard deviation of the error for the ANN-based

AoA estimation in relation to the vane measurements were considerably smaller than that of the single pressure sensor estimate (0.30° vs −0.92° for the mean error and 1.77° vs 2.66° for the error standard deviation). The error distribution shows two peaks for both the single pressure sensor estimate and the ANN estimate. This appeared to be due to a zeroing error with the AoA vane in one of the validation flights indicating that the results presented are likely to be an underestimate of the accuracy of the AoA estimates.

To test if any sensor was particularly influential in the ANN estimate of AoA, a series of tests were conducted where the ANN was trained and validated with each individual sensor signal excluded from the data in turn. It was found that all the ANN's using six sensor ports performed with a similar level of accuracy as the full seven sensor ANN, with the worst performing ANN having a RMS error of 2.25° compared to 1.79° for the full sensor ANN (Table 3). This was also true when only looking at the post-stall performance of the networks. This indicates that no single sensor signal was essential for good performance of the ANN estimate of AoA.

Figure 14b shows the ANN-based airspeed estimation error distribution. The estimation performance is similar for both wind tunnel and flight testing training data, but degrades as one goes from training data to the outdoor validation datasets.

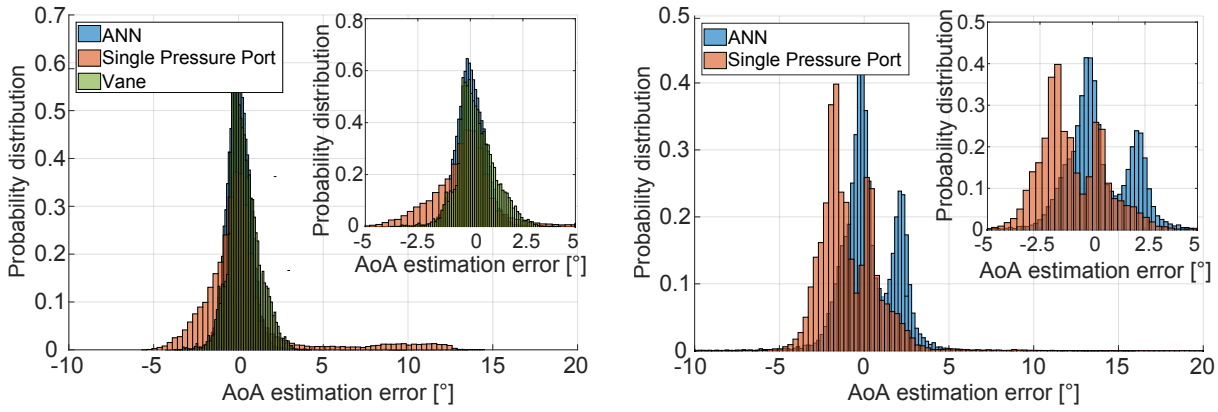

Fig. 13 Angle of attack estimation error distribution for: (a) wind tunnel and (b) outdoor flights data sets.

Table 2 Estimation RMS error statistics

Data set	AoA RMS error [°]						V RMS error [m s^{-1}]	
	Vane	Single PS	ANN	Vane	Single PS	ANN	ANN	
	Overall			AoA > 10°			Overall	AoA > 10°
WT training	0.949	2.934	0.933	1.167	4.694	1.243	0.274	0.332
Outdoors training	-	1.762	0.776	-	4.642	3.852	0.402	1.226
Outdoors validation	-	2.813	1.792	-	11.409	3.681	0.758	1.644

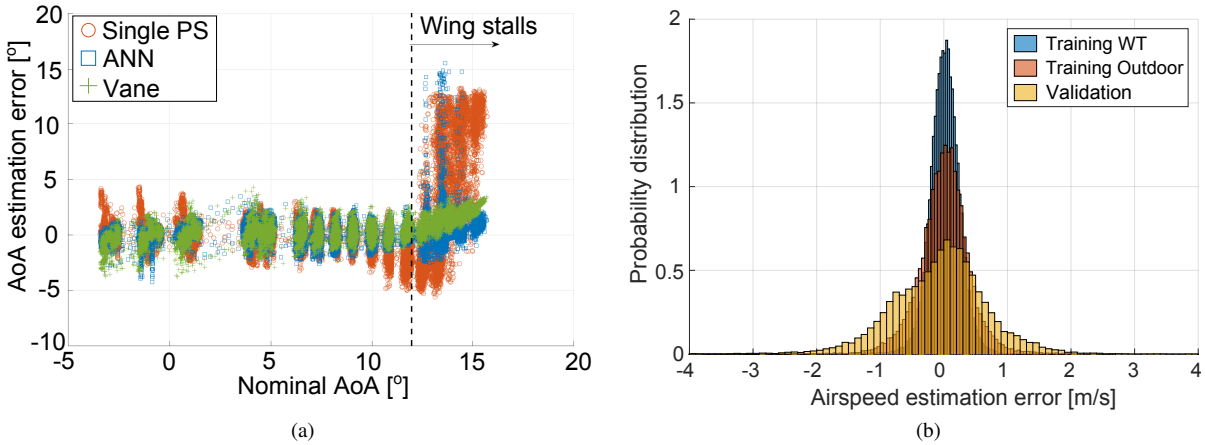

(a) (b)

Fig. 14 Estimation performance: (a) angle of attack wind tunnel data comparison and (b) ANN-based airspeed estimation error distribution.

Table 3 AoA estimation errors with one sensor removed

Sensor removed	Training		Validation	
	Overall RMSE [°]	AoA>10° RMSE	Overall RMSE [°]	AoA>10° RMSE
None	0.877	1.287	1.792	3.680
PS01	1.123	1.377	1.789	2.977
PS02	0.882	1.280	1.921	3.974
PS03	0.739	1.049	1.766	3.870
PS04	1.046	1.519	1.773	3.159
PS05	0.905	1.397	2.212	3.692
PS06	0.905	1.392	2.246	5.637
PS07	1.203	1.927	1.556	4.513

VI. Discussion

Using wind tunnel testing the characteristics of a chord-wise distributed array of pressure sensors were measured. Simultaneously a conventional airspeed sensor and an AoA vane were also characterised and calibrated. The same fixed wing UAS was then flight tested, firstly manually piloted through a series of pitching manoeuvres, then in a series of automated manoeuvres based on closed loop feed back using an estimate of AoA from a single pressure port. Post-processing of wind tunnel and flight testing data was then used to train an ANN to estimate the AoA and V of the UAS based on signals from all of the pressure ports in the array.

A. AoA and V estimation

During wind tunnel testing it was found that the signal from a single port pressure at 3% chord could be used to provide a reasonable estimate of AoA pre-stall (AoA < 10°) when normalised by dynamic pressure, but that post-stall this signal fluctuated greatly (Fig. 5b). This pattern of behaviour is likely to be due to the position of the suction peak on

the upper surface of the wing being located close to 3% chord. Up to stall the C_p of the peak would be expected to scale linearly with AoA. Once the wing had stalled the flow appeared to be separated near the leading edge, with the pressure becoming unsteady in the region of separated flow. This agrees with previous studies where pressure ports near the leading edge were shown to provide signals that have a strong relationship with AoA [6, 8], which then breaks down in stall conditions [10].

An ANN using the signals from all of the pressure ports was able to provide reliable estimates of AoA throughout the range of AoA tested in the wind tunnel (−4° to 16°) with an RMS error practically equal to that of the AoA vane (0.93° vs 0.95°). This level of performance is comparable to other wind tunnel studies where wing mounted arrays of sensors have been used to estimate AoA [6, 11, 13–15]. The ANN estimate of AoA was comparable to the vane estimate and appeared to provide a similar estimate to the vane post-stall (Fig. 14a). It was found that the estimate of post-stall AoA was not reliant on the signal from pressure port 7, the only pressure port on the lower surface of the wing. All of the signals from the upper surface ports became unsteady in the post-stall region, while port 7 remained steady. However, when port 7 was excluded from the data set used to train and validate the ANN a reasonable estimate of the AoA was still obtained (Table 3). This indicates that the ANN was able to cope with the noise in the unsteady pressure signals to extract a reasonable approximation of the AoA. Previous studies with pressure ports mounted on the aircraft nose cone have been able to estimate AoA in the post-stall region [21–23], but studies with wing mounted ports have not explored this region in the context of estimating the AoA based on the unsteady signals using an ANN. These results indicate that wing mounted pressure ports may be able to be used to give a useful estimate of AoA even once the wing has stalled.

During outdoor flight testing the single pressure port estimate of AoA was again reasonable pre-stall, but not so post-stall (Table 2). The ANN AoA estimate was comparable to the vane AoA estimate. The ANN AoA outdoor validation RMS error (1.79°) was larger than the wind tunnel (0.93°) and the outdoor training set error (0.78°), this is likely to be due to the increased turbulence present outdoors and the validation flight conditions falling outside of the range of the training data at times. During the outdoor test flights when the aircraft was deliberately manually stalled (Fig. 9) the three estimates of AoA diverged during stall. The divergence of the single pressure port estimate was expected due to flow separation as was seen in wind tunnel testing. The ANN estimated a markedly higher AoA than the vane during the abrupt stall, unlike during less abrupt stalls that occurred during close-loop flight tests (Fig. 10) where it agreed more closely with the vane measurement. This may have been due to the pressure signal having a faster dynamic response than the AoA vane which has a certain level of inertia as can be seen by its smoother response in Fig. 9 and Fig. 10.

The performance of an ANN in estimating airspeed based all of the distributed pressure port information was assessed against the airspeed measurements from a Pitot tube mounted on the wing close to the wing insert. This ANN also had a level of performance comparable to other wind tunnel studies with wing mounted sensors [6, 11, 13–15]. In outdoor test flights there were occasions when the ANN and Pitot estimates of V differed significantly (Fig. 10 and

Table 2), this occurred when the aircraft was flying at a high AoA ($> 10°$) and is thought to be due to the high angle of incidence of the pitot tube which led to an under estimate of the dynamic pressure. This effect was also seen in wind tunnel testing. This suggests that ANN estimates of V based on distributed flow sensing may have an advantage over conventional pitot based measurements by incorporating high AoA effects.

These results show the feasibility of using a distributed array of flow sensors on the wing of a UAS to estimate AoA and airspeed. This has previously been demonstrated in wind tunnel studies, but data from flight tests outdoors is sparse. Previous flight tests with pressure ports on the nose cone of aircraft [22, 24] have shown the feasibility of these systems, also known as Flush Air Data Systems (FADS) to estimate a range of aerodynamic parameters including AoA and V. The potential advantages of having the flow sensor array on the wing, rather that the nose cone, is that direct measurement of flow states such as stall are possible, while still providing estimates of the vehicles overall air velocity vector. However, it is likely some estimates such as side-slip angle may be more accurate based on measurements made on the nose cone than the wing. Alternatively parameter estimates could be optimised by placing sensors in a range of locations on the aircraft [11].

B. AoA based attitude control

The closed loop flight tests based on holding a set AoA as estimated using the signal from the 3% chord pressure port showed that it is possible to control the attitude of an aircraft with reference to AoA rather than pitch angle as is done conventionally. A potential advantage of using an AoA reference for attitude control is that the attitude of the aircraft is referenced relative to the airspeed vector of the aircraft rather than gravity. This means that the aircraft is referenced to the relative direction of the airflow including the effect of wind. This has potential advantages when operating in strong wind fields, such as can occur close to terrain and buildings. For instance, there is potential for the control system to avoid commanding an attitude that could cause the aircraft to stall if the wind field has a strong vertical component. AoA based control could also potentially help mitigate some of the effects of unsteady wind by acting to maintain a constant lift rather than constant pitch attitude, as demonstrated by the climb rate results.

C. Future development

The results shown here are for a system where pressure sensing has been used in place of a conventional IMU for longitudinal attitude control to demonstrate the feasibility of the concept. In future developments, the idea would be to supplement the information available from IMU and GPS sensors with the airflow information available from the pressure sensors. This has the potential to allow the usable flight envelop of a UAS to be extended. For example, the flow sensors can be used to detect flow separation and stall in different regions of the wing, offering the potential to operate much closer to the stall limits of the aircraft. Previous work [7, 25], has used manually selected thresholds for properties of the pressure distribution to detect stall, but it would seem that an ANN approach would also be well

suited for this task if a training set with direct measurements of stall state were available (which was not the case in this work). Taking the idea of stall detection further, the controller could intentionally stall the aircraft during extreme manoeuvres and then recover by sensing when the flow has reattached to the wing. Due to the chaotic nature of stalled flow, reattachment is difficult to predict, but quite feasible to measure directly with flow sensors.

A further extension of this concept would be to incorporate more sensors into UAS wings and tails to measure the distribution of flow across the wing span and on the tail planes. This would give the potential to also use flow sensors as part of the lateral attitude control system. Having a more distributed array with a greater number of sensors also offers the opportunity to monitor the flow state over different parts of the wing. This could offer many advantages for the control of highly flexible winged aircraft, where the flow state has the potential to be very different over different parts of the wing due to aero-elastic effects [26]. The type of arrangement would be very similar to that seen in biological flyers, where distributed force and flow sensors appear to be used with highly flexible wings where aero-elastic effects play a major role in flight performance and control.

D. Conclusions

This study presented both a new method of sensing the angle-of-attack of a small UAS and successfully used this additional signal for closed-loop flight control. A single pressure sensor located near the leading edge of the wing can be used to measure angle of attack in sub-stall conditions via a characterisation using wind-tunnel testing. This method can be used to control the longitudinal axis of a UAS such that a set AoA is maintained via feedback control. A second method of estimating AoA, using artificial neural networks, used of the full array of chord-wise pressure ports and yielded a more robust estimate of AoA and additionally estimated velocity. The ANN method could also provide an improved measurement of AoA in the stall region when compared to the single port method.

This work moved beyond simulation and controlled laboratory tests and proved the system under real-world conditions with experimental validation from outdoor flight testing. Future work will more closely integrate the ANN estimation method into the flight control system and expand the quantity and distribution of pressure ports, with an aim of robustly maintaining stability at the edges of the flight envelope.

Acknowledgements

The authors would like to thank Mr Lee Winter from the University of Bristol wind tunnel laboratory, for his invaluable support and work during the assembly of the pressure sensing system. The work presented in this paper was partially funded by the Defence Science and Technology Laboratory (DSTL), under contract number DSTLX-1000097967. This project has received funding from the European Research Council (ERC) under the European Union's Horizon 2020 research and innovation programme (grant agreement No 679355).

References

[1] Roth, M., "Review of atmospheric turbulence over cities," *Quarterly Journal of the Royal Meteorological Society*, Vol. 126, No. 564, 2000, pp. 941–990. doi:10.1002/qj.49712656409.

[2] Mohamed, A., Clothier, R., Watkins, S., Sabatini, R., and Abdulrahim, M., "Fixed-wing MAV attitude stability in atmospheric turbulence, part 1: Suitability of conventional sensors," *Progress in Aerospace Sciences*, Vol. 70, 2014, pp. 69–82. doi: 10.1016/j.paerosci.2014.06.001.

[3] Brown, R. E., and Fedde, M. R., "Airflow sensors in the avian wing," *Journal of Experimental Biology*, Vol. 179, No. 1, 1993, pp. 13–30.

[4] Sterbing-D'Angelo, S., Chadha, M., Chiu, C., Falk, B., Xian, W., Barcelo, J., Zook, J. M., and Moss, C. F., "Bat wing sensors support flight control," *Proceedings of the National Academy of Sciences*, Vol. 108, No. 27, 2011, pp. 11291–11296. doi:10.1073/pnas.1018740108.

[5] Taylor, G. K., and Krapp, H. G., "Sensory systems and flight stability: what do insects measure and why?" *Advances in insect physiology*, Vol. 34, 2007, pp. 231–316. doi:10.1016/S0065-2806(07)34005-8.

[6] Samy, I., Postlethwaite, I., Gu, D.-W., and Green, J., "Neural-network-based flush air data sensing system demonstrated on a mini air vehicle," *Journal of Aircraft*, Vol. 47, No. 1, 2010, pp. 18–31. doi:10.2514/1.44157.

[7] Yeo, D., Atkins, E. M., and Bernal, L. P., "Aerodynamic Sensing for a Fixed Wing UAS Operating at High Angles of Attack," *AIAA Atmospheric Flight Mechanics Conference*, 2012. doi:10.2514/6.2012-4416.

[8] Shen, H., Xu, Y., and Remeikas, C., "Pitch control of a micro air vehicle with micropressure sensors," *Journal of Aircraft*, Vol. 50, No. 1, 2012, pp. 239–248. doi:10.2514/1.c031894.

[9] Marino, M., Ravi, S., and Watkins, S., "Optimum location of pressure measurments around a wing as a dynamic control input in smooth and turbulent conditions," *28th International Congress of the Aeronautical Sciences*, Vol. 2, 2012, pp. 955–962.

[10] Mohamed, A., Watkins, S., Fisher, A., Marino, M., Massey, K., and Clothier, R., "Bioinspired Wing-Surface Pressure Sensing for Attitude Control of Micro Air Vehicles," *Journal of Aircraft*, Vol. 52, No. 3, 2015, pp. 829–838. doi:10.2514/1.C032805.

[11] Laurence III, R. J., Argrow, B. M., and Frew, E. W., "Wind tunnel results for a distributed flush airdata system," *Journal of Atmospheric and Oceanic Technology*, Vol. 34, No. 7, 2017, pp. 1519–1528. doi:10.1175/JTECH-D-16-0242.1.

[12] Thompson, K., Xu, Y., and Dickinson, B. T., "Aerodynamic moment model calibration from distributed pressure arrays," *Journal of Aircraft*, Vol. 54, No. 2, 2017, pp. 716–723. doi:10.2514/1.c033898.

[13] Fei, H., Zhu, R., Zhou, Z., and Wang, J., "Aircraft flight parameter detection based on a neural network using multiple hot-film flow speed sensors," *Smart Materials and Structures*, Vol. 16, No. 4, 2007, p. 1239. doi:10.1088/0964-1726/16/4/035.

[14] Que, R., and Zhu, R., "Aircraft aerodynamic parameter detection using micro hot-film flow sensor array and BP neural network identification," *Sensors*, Vol. 12, No. 8, 2012, pp. 10920–10929. doi:10.3390/s120810920.

[15] Magar, K. T., Reich, G. W., Kondash, C., Slinker, K., Pankonien, A. M., Baur, J. W., and Smyers, B., "Aerodynamic parameters from distributed heterogeneous CNT hair sensors with a feedforward neural network," *Bioinspiration & Biomimetics*, Vol. 11, No. 6, 2016, p. 066006. doi:10.1088/1748-3190/11/6/066006.

[16] Pankonien, A. M., Magar, K. S. T., Beblo, R. V., and Reich, G. W., "Gust prediction via artificial hair sensor array and neural network," *A Tribute Conference Honoring Daniel Inman*, Vol. 10172, International Society for Optics and Photonics, 2017, p. 101720F. doi:10.1117/12.2257243.

[17] Mohamed, A., Abdulrahim, M., Watkins, S., and Clothier, R., "Development and Flight Testing of a Turbulence Mitigation System for Micro Air Vehicles," *Journal of Field Robotics*, Vol. 33, No. 5, 2016, pp. 639–660. doi:10.1002/rob.21626.

[18] Thompson, R., Evers, J., and Stewart, K., "Attitude Control Augmentation Using Wing Load Sensing - A Biologically Motivated Strategy," *AIAA Atmospheric Flight Mechanics Conference*, 2010. doi:10.2514/6.2010-7936.

[19] Shen, H., Xu, Y., and Dickinson, B. T., "Micro Air Vehicle's Attitude Control Using Real-Time Pressure and Shear Information," *Journal of Aircraft*, Vol. 51, No. 2, 2014, pp. 661–671. doi:10.2514/1.C032375.

[20] Araujo-Estrada, S. A., Salama, F., Greatwood, C. M., Wood, K. T., Richardson, T. S., and Windsor, S. P., "Bio-inspired Distributed Strain and Airflow Sensing for Small Unmanned Air Vehicle Flight Control," *AIAA Guidance, Navigation, and Control Conference*, 2017. doi:10.2514/6.2017-1487.

[21] Crowther, W., and Lamont, P., "A neural network approach to the calibration of a flush air data system," *The Aeronautical Journal*, Vol. 105, No. 1044, 2001, pp. 85–95. doi:10.1017/S0001924000011532.

[22] Rohloff, T. J., Angeles, L., Angeles, L., Whitmore, S. A., and Catton, I., "Air data sensing from surface pressure measurements using a neural network method," *AIAA journal*, Vol. 36, No. 11, 1998, pp. 2094–2101. doi:10.2514/3.14090.

[23] Martin, I., Ben, C., Voget, N., and Moormann, D., "Design and Evaluation of a Realtime, Microcontroller Based Gust Sensing System for a Small Unmanned Aerial Vehicle," *33rd AIAA Aerodynamic Measurement Technology and Ground Testing Conference*, 2017. doi:10.2514/6.2017-3235.

[24] Quindlen, J., and Langelaan, J., "Flush air data sensing for soaring-capable UAVs," *51st AIAA Aerospace Sciences Meeting Including the New Horizons Forum and Aerospace Exposition*, 2013, pp. 1–17. doi:10.2514/6.2013-1153.

[25] Yeo, D., Henderson, J., and Atkins, E., "An Aerodynamic Data System for Small Hovering Fixed-Wing UAS," *AIAA Guidance, Navigation, and Control Conference*, 2009. doi:10.2514/6.2009-5756.

[26] Patil, M. J., Hodges, D. H., and S. Cesnik, C. E., "Nonlinear Aeroelasticity and Flight Dynamics of High-Altitude Long-Endurance Aircraft," *Journal of Aircraft*, Vol. 38, No. 1, 2001, pp. 88–94. doi:10.2514/2.2738.